

Size of the group IVA iron meteorite core: Constraints from the age and composition of Muonionalusta

Nicholas A. Moskovitz^{a,*}, Richard J. Walker^b

^a*Carnegie Institution of Washington, Department of Terrestrial Magnetism, 5241 Broad Branch Road, Washington, DC 20015, USA*

^b*University of Maryland, Department of Geology, College Park, MD 20742*

Abstract

The group IVA fractionally crystallized iron meteorites display a diverse range of metallographic cooling rates. These have been attributed to their formation in a metallic core, approximately 150 km in radius, that cooled to crystallization in the absence of any appreciable insulating mantle. Here we build upon this formation model by incorporating several new constraints. These include (i) a recent U-Pb radiometric closure age of <2.5 Myr after solar system formation for the group IVA iron Muonionalusta, (ii) new measurements and modeling of highly siderophile element compositions for a suite of IVAs, and (iii) consideration of the thermal effects of heating by the decay of the short-lived radionuclide ^{60}Fe . Our model for the thermal evolution of the IVA core suggests that it was approximately 50 - 110 km in radius after being collisionally exposed. This range is due to uncertainties in the initial abundance of live ^{60}Fe incorporated into the IVA core. Our models define a relationship between cooling rate and closure age, which is used to make several predictions that can be tested with future measurements. In general,

*Corresponding author: nmoskovitz@dtm.ciw.edu

our results show that diverse cooling rates and early U-Pb closure ages can only coexist on mantle-free bodies and that energy released by the decay of ^{60}Fe reduces the core size necessary to produce diverse metallographic cooling rates. The influence of ^{60}Fe on cooling rates has largely been neglected in previous core formation models; accounting for this heat source can affect size estimates for other iron meteorite cores that cooled to crystallization in the presence of live ^{60}Fe . Candidates for such a scenario of early, mantle-free formation include the iron IIAB, IIIAB and IVB groups.

Keywords: iron meteorites, planetary differentiation, early Solar System

1. Introduction

Amongst the oldest melted rocks in the solar system, fractionally crystallized iron meteorites provide insight on the early stages of planet formation. These meteorites are interpreted as fragments of cores from planetesimals that melted and subsequently differentiated due to heating by the decay of short-lived radioactive isotopes like ^{26}Al and ^{60}Fe (Mittlefehldt et al., 1998; Goldstein et al., 2009; Moskovitz and Gaidos, 2011). Though these meteorites are highly evolved, differences in their composition and structure provide a basis for classification (Haack and McCoy, 2005). Fourteen well-defined groups of iron meteorites have been identified, most of which are thought to represent the cores of distinct parent bodies (Goldstein et al., 2009). While the classification of these groups is generally agreed upon, details of their formation, such as parent body size, are less certain.

The origin of the group IVA iron meteorites has long been debated due to several unusual properties (Willis and Wasson, 1978; Rasmussen et al., 1995;

16 Haack et al., 1996; Scott et al., 1996; Wasson and Richardson, 2001; Ruzicka
 17 and Hutson, 2006; Wasson et al., 2006; Yang et al., 2008). First, they display
 18 the widest range of metallographic cooling rates (100-6600 K/Myr) of any
 19 iron meteorite group (Yang et al., 2008). These rates were recorded during
 20 the formation of the Widmanstätten pattern (WP, a structure of interleaved
 21 bands of kamacite and taenite) as the core cooled from 1000 to 700 K. In
 22 addition, the diameters of cloudy zone (CZ) particles at the boundaries of
 23 taenite crystals suggest that the IVA cooling rates between 600 to 500 K
 24 varied by a factor of fifteen (Yang et al., 2007). Second, several IVAs contain
 25 silicate inclusions, which have been explained through a host of impact and
 26 melt evolution scenarios (Ulff-Møller et al., 1995; Haack et al., 1996; Ruzicka
 27 and Hutson, 2006; Wasson et al., 2006; McCoy et al., 2011). Third, they are
 28 significantly depleted in moderately volatile siderophile elements relative to
 29 chondrites and other iron groups (Wasson and Richardson, 2001; Yang et al.,
 30 2008; McCoy et al., 2011). Lastly, though not exclusive to the IVAs, their
 31 trace element abundances are consistent with sampling a majority of their
 32 parent core’s fractional crystallization sequence (Scott et al., 1996; Wasson
 33 and Richardson, 2001; Ruzicka and Hutson, 2006; McCoy et al., 2011).

34 One formation scenario that reasonably explains these properties (see
 35 Yang et al. (2008) and Ruzicka and Hutson (2006) for overviews of other mod-
 36 els) suggests that the differentiated IVA parent body was originally ~ 1000
 37 km in diameter prior to a hit-and-run collision with a comparably massive
 38 proto-planet (Asphaug et al., 2006; Yang et al., 2007). This collision released
 39 a string of metal-rich fragments that eventually cooled to crystallization with-
 40 out the insulating effects of an overlying silicate mantle. In this scenario, the

41 isolated core that would eventually be disrupted to produce the IVA me-
42 teorites must have been ~ 300 -km in diameter to reproduce the wide range
43 of metallographic cooling rates. A lack of insulating mantle is necessary to
44 achieve rapid cooling (>1000 K/Myr) near the surface and the large size
45 ensures that the center of the body cools slowly (~ 100 K/Myr).

46 This formation scenario merits revisiting in light of a recent U-Pb age for
47 the IVA Muonionalusta, which indicates system closure (i.e. cooling below
48 ~ 600 K) at 4565.3 ± 0.1 Ma (Blichert-Toft et al., 2010). This is the earliest
49 measured age for any fractionally crystallized iron. It falls only ~ 1 Myr after
50 the basaltic angrite Asuka 881394, the oldest differentiated rock in the Solar
51 System (Wadhwa et al., 2009), and is less than 2.5 Myr after the formation of
52 CAIs (calcium-aluminum-rich inclusions), generally considered to be the first
53 solids to condense from the solar nebula. The aim of this paper is build upon
54 the IVA formation model first presented in Yang et al. (2007) by taking into
55 account newly available constraints on the evolution of the IVA parent core.
56 In §2 we present a fractional crystallization model to provide context for the
57 origin of Muonionalusta relative to other IVAs. In §3 we outline a thermal
58 conduction model that includes heating by the decay of ^{60}Fe . This thermal
59 model and the result of the fractional crystallization calculation are used to
60 constrain the size of the IVA core and make predictions for the closure ages
61 of other IVAs (§4). In §5 we discuss the sensitivity of our results to various
62 assumptions inherent to the thermal model. In §6 we summarize and discuss
63 the broader implications of this work.

64 2. Model of IVA Fractional Crystallization

65 To estimate the extent of fractional crystallization required to produce
66 Muonionalusta we model the IVA system assuming 3% and 0.1% initial S and
67 P, respectively, using an approach similar to that of Walker et al. (2008) for
68 the IVB irons (Fig. 1). Initial Re and Os concentrations of 295 and 3250 ppb,
69 respectively, are estimated for the IVA parental melt. Details of this model
70 are provided in McCoy et al. (2011). For these starting parameters, the Re
71 and Os concentrations of Muonionalusta are attained after $\sim 60\%$ fractional
72 crystallization, assuming that it has a composition consistent with an equi-
73 librium solid. Appropriate concentrations are attained after 50% fractional
74 crystallization if Muonionalusta has a composition consistent with that of the
75 evolving IVA liquid. Mixtures of solid and liquid compositions are achieved
76 by intermediate extents of fractional crystallization. This result is generally
77 consistent with the model of Wasson and Richardson (2001), who generated
78 a composition similar to Muonionalusta after $\sim 40\%$ and $\sim 55\%$ fractional
79 crystallization, using Au versus Ir and As versus Ir plots, respectively. It is
80 also consistent with Yang et al. (2008) who showed that an iron with 8.4%
81 Ni-content like Muonionalusta would crystalize after $\sim 60\%$ solidification of
82 a core with initial 3 wt.% S.

83 For an inwardly crystallizing core, as expected for the IVA parent (Haack
84 and Scott, 1992; Ruzicka and Hutson, 2006; Yang et al., 2008), these data
85 suggest that Muonionalusta formed between approximately 80-70% of the
86 parent body radius, with 70% representing the best fit to our data (Fig. 1).
87 This sub-surface origin is consistent with Muonionalusta's Ni abundance (an
88 indicator of cooling rate), which is intermediate to other IVAs (Blichert-Toft

et al., 2010; Yang et al., 2008).

3. Thermal Conduction Model

Because of the need for rapid cooling, our model, like that of Yang et al. (2007), begins with a body without any insulating silicate mantle. This model is based on the 1D thermal conduction equation (Moskovitz and Gaidos, 2011) and assumes a metallic sphere with the following properties: density 7500 kg/m^3 , thermal conductivity 50 W/m/K , specific heat 400 J/kg/K , initial uniform temperature of 1750 K , and a fixed boundary temperature of 200 K . These material properties are within 20% of those used in other thermal models for differentiated bodies and are generally applicable to iron alloys (Ghosh and McSween, 1998, 1999; Hevey and Sanders, 2006; Yang et al., 2007; Moskovitz and Gaidos, 2011). The initial and boundary temperatures match those used by Yang et al. (2007). We use a fixed-temperature, Dirichlet boundary condition, which is simpler to implement than a radiative boundary condition, does not introduce significant error for the range of temperatures in which we are interested, and produces results no different from a radiative boundary for all radii up to a few km from the surface (Ghosh and McSween, 1998; Yang et al., 2007; Moskovitz and Gaidos, 2011). The boundary at 200 K is an approximation for the ambient temperature in the solar nebula (Yang et al., 2007). In §5.2 we show that our results are insensitive to a reasonable range of assumed initial and boundary temperatures.

One difference between our model and those of previous investigators is that we have considered heating by the decay of ^{60}Fe . Previous models (e.g. Haack et al., 1990; Yang et al., 2008) assumed that no heat sources

113 were available after ^{26}Al caused melting and differentiation. However, the
 114 solar system's initial abundance of ^{60}Fe relative to its stable isotope ^{56}Fe is
 115 not precisely known. Therefore we present two scenarios for the IVA parent
 116 core: one in which the core thermally evolves with a maximum possible
 117 abundance of ^{60}Fe and the second in which no ^{60}Fe is present. These scenarios
 118 produce lower and upper limits respectively to the size of the IVA core. After
 119 accounting for a recently revised half-life of 2.62 Myr and properly reduced
 120 mass spectrometry results, a reasonable maximum for the ratio $^{60}\text{Fe}/^{56}\text{Fe}$ at
 121 the time of CAI formation is 4×10^{-7} (Rugel et al., 2009; Mishra et al.,
 122 2010; Telus et al., 2011; Ogliore et al., 2011). For the maximum heating
 123 case, we adopt this half-life and abundance, along with a decay energy of
 124 3.04 MeV and an Fe mass fraction of 90% for the IVA parent body (Ghosh
 125 and McSween, 1998; Mittlefehldt et al., 1998). This case assumes that all of
 126 the chondritic ^{60}Fe is sequestered into the core, again resulting in an upper
 127 limit on the energy available from radiogenic decay.

128 Other studies suggest that the initial $^{60}\text{Fe}/^{56}\text{Fe}$ ratio was up to several
 129 orders of magnitude lower and/or heterogeneously distributed in the solar
 130 nebula, resulting in reservoirs largely depleted in ^{60}Fe (Chen et al., 2009;
 131 Quitte et al., 2010; Spivak-Birndorf et al., 2011; Tang and Dauphas, 2011).
 132 To bracket the range of possible abundances we also consider the thermal
 133 evolution of the IVA parent core in the absence of any ^{60}Fe . This minimum-
 134 ^{60}Fe model is analogous to that presented by Yang et al. (2008), though we
 135 now use this model to match the additional constraints of age and formation
 136 radius for Muonionalusta. The specific lower limit for ^{60}Fe is not critically
 137 important; once $^{60}\text{Fe}/^{56}\text{Fe}$ drops more than an order of magnitude below the

upper limit, i.e. $\leq 5 \times 10^{-8}$, the energy available from the decay of ^{60}Fe would have been insignificant in the overall thermal budget of the IVA parent body.

The thermal model assumes that the IVA core was fully formed at 4567.7, a weighted mean of recently measured CAI ages (Jacobsen et al., 2008; Burkhardt et al., 2008). The statistical uncertainty on this weighted mean is 0.3 Myr, though systematic errors could be as large as 1 Myr (see §5.4, Amelin et al., 2010). This assumption requires that accretion, differentiation and exposing of the IVA core occurred much faster than the $\sim 10^6$ -year timescales for ^{60}Fe heating and conductive cooling (Rugel et al., 2009; Moskovitz and Gaidos, 2011). This is consistent with hydrodynamic simulations of planetesimal formation in turbulent proto-planetary disks that show bodies as large as 1000 km accreted in much less than 10^3 years (Johansen et al., 2007). In §5.5 we show that this nearly instantaneous accretion anytime within 1.5 Myr of CAI formation, a limit for fractionally crystallized iron cores, does not affect our size estimates for the IVA core (Haack and McCoy, 2005; Qin et al., 2008). The assumed initial temperature of 1750 K at 4567.7 Ma is unphysical, however a variety of heat sources (e.g. ^{26}Al decay and impacts) could have contributed to the global heating of bodies hundreds of km in size (Keil et al., 1997; Moskovitz and Gaidos, 2011). These heat sources would have been relevant on timescales of $10^5 - 10^6$ years.

4. Models of the IVA Core

Figure 2 shows how temperature varies as a function of cooling rate in two different exposed cores. These temperature profiles are shown for a range of depths, from the center of the body up to 97% of the radius R . The top

162 panel (A) depicts a case with maximum $^{60}\text{Fe}/^{56}\text{Fe}=4 \times 10^{-7}$ and $R = 50$ km;
163 the bottom panel (B) depicts a core with no ^{60}Fe and $R = 130$ km.

164 The release of energy from the decay of ^{60}Fe prolongs cooling and reduces
165 cooling rates. Thus, the body in Figure 2A, which is only 50 km in radius,
166 exhibits cooling rates as small as 140 K/Myr at its center during the forma-
167 tion of the Widmanstätten pattern (1000-700 K) and a range of rates during
168 the formation of cloudy zone particles (600-500 K) that is consistent with
169 measurements. Furthermore, WP cooling rates at $0.7R$ are as expected for
170 Muonionalusta based on rates measured for its compositional analog Seneca
171 Township (300-1200 K/Myr, Yang et al., 2008). If no ^{60}Fe were present on
172 a body this small then none of these constraints would be met: the lowest
173 cooling rates during WP formation would be an order of magnitude larger,
174 the CZ rates would only vary by a factor of 10, and the WP cooling rates
175 at $0.7R$ would be larger than those measured for Seneca Township. Smaller
176 bodies with this ^{60}Fe abundance cool too quickly to reproduce the low end
177 of the IVA range of WP rates. As such, a radius of 50 km is a lower limit for
178 a core to be able to reproduce the IVA cooling rate data.

179 An upper limit for the size of the IVA core is depicted in Figure 2B. In
180 this case, no ^{60}Fe is present, thus requiring $R = 130$ km to achieve slow
181 cooling (~ 100 K/Myr) near the center. A body with these properties meets
182 the WP, CZ and Seneca cooling rate constraints. Although a larger body
183 would produce the necessary range of WP and CZ rates, the cooling rates
184 at $0.7R$ would be too slow (< 100 K/Myr) for Seneca Township. Therefore,
185 the cooling rates modeled in Figure 2 bracket the size of the IVA core to
186 somewhere between 50 and 130 km.

187 The age of Muonionalusta further constrains the size of the IVA core.
 188 Figure 3 shows the times at which different depths in exposed cores reach U-
 189 Pb isotopic closure at 600 K (Blichert-Toft et al., 2010). The two panels again
 190 correspond to $^{60}\text{Fe}/^{56}\text{Fe}=4\times 10^{-7}$ (A) and $^{60}\text{Fe}/^{56}\text{Fe}=0$ (B) and produce lower
 191 and upper size limits respectively. For the former, Muonionalusta would
 192 crystallize at 4565.3 Myr in a core with a radius of 55 km (i.e. where the bold
 193 curve intersects the shaded region). For the later, the age of Muonionalusta
 194 is reproduced for a core 110 km in radius.

195 Matching both the cooling rates (Fig. 2) and the U-Pb age at the ex-
 196 pected depth of Muonionalusta's origin (Fig. 3) suggests that the IVA core
 197 was between 50 and 110 km in radius, depending upon the assumed initial
 198 abundance of ^{60}Fe . Below this lower limit the entire body would reach U-Pb
 199 closure within 2.5 Myr (Fig. 3A), requiring that Muonionalusta come from
 200 the center of the IVA core. This would unreasonably preclude cooling rates
 201 slower than the 500 K/Myr inferred for Muonionalusta (Blichert-Toft et al.,
 202 2010). Conversely, a core with $R>110$ km would not reach U-Pb closure in
 203 <2.5 Myr at $0.7R$ (Fig. 3B). We adopt $R=50$ km as a lower limit rather than
 204 55 km because several of the assumptions in these models hasten cooling and
 205 thus demand an increase in size to produce slow ~ 100 K/My cooling (see
 206 §5).

207 In these models, size and ^{60}Fe abundance are degenerate properties whose
 208 variation produces a series of solutions that fulfill the cooling rate and age
 209 constraints. The examples in Figures 2 and 3 are end-member cases that
 210 bracket the range of possibilities. If the initial ^{60}Fe abundance in the IVA
 211 parent core were known, then it is possible to predict a specific relationship

212 between U-Pb closure age and cooling rate. For example, a given depth
 213 profile in Figure 2 records a range of cooling rates between 1000-700 K and a
 214 U-Pb closure age at 600 K. Table 1 presents predicted ages for several IVAs by
 215 assuming that the mean cooling rate measured for each sample corresponds
 216 to the rate midway between 1000 and 700 K. These predictions are specific
 217 to the case of $R=50$ km and $^{60}\text{Fe}/^{56}\text{Fe}=4 \times 10^{-7}$ and are simply intended to
 218 highlight several implications of this formation model.

219 First, the results in Table 1 predict a wide range of U-Pb closure ages from
 220 4564.0 - 4567.5 Ma. This range of several Myr is a general outcome of these
 221 models, irrespective of the assumed ^{60}Fe abundance, and is resolvable with
 222 the current precision of U-Pb dating techniques (Blichert-Toft et al., 2010).
 223 None of our models produce rates less than ~ 140 K/Myr and thus cannot
 224 predict the closure ages of the four most chemically evolved IVAs (Duchesne,
 225 Chinautla, New Westville and Steinbach), though it is likely they reached
 226 U-Pb closure after 4654 Ma. We do not view this as a significant failure
 227 of the model considering the large uncertainties and many assumptions that
 228 have been made (see §5). Varying input parameters such as the specific heat
 229 could reduce the calculated cooling rates to the 100 K/My that is measured
 230 for Duchesne.

231 Second, the correlation between closure age and cooling history pre-
 232 dicts cooling rates for Muonionalusta. For example, when $R=50$ km and
 233 $^{60}\text{Fe}/^{56}\text{Fe}=4 \times 10^{-7}$, Muonionalusta's closure age suggests cooling rates be-
 234 tween 290-940 K/Myr, which by design are similar to the range of rates for
 235 Seneca Township (Yang et al., 2008).

236 Lastly, this formation model predicts that IVAs with the fastest cooling

237 rates will have the oldest U-Pb closure ages. In the example shown in Table
 238 1, the predicted ages for samples like La Grange and Bishop Canyon are
 239 only a few hundred thousand years separated from the formation of CAIs. If
 240 this formation scenario is correct, then these IVAs may represent the oldest
 241 differentiated rocks in the Solar System.

242 5. Assumptions in the Thermal Model

243 5.1. Neglected processes

244 The release of latent heat during crystallization, the temperature depen-
 245 dence of specific heat, and the effect of an insulating layer have been neglected
 246 in these models. The net latent heat available in the Fe-Ni-S system is 270
 247 kJ/kg (Haack et al., 1990), which is less than the total energy released by
 248 the decay of ^{60}Fe when the initial $^{60}\text{Fe}/^{56}\text{Fe} > 6 \times 10^{-8}$. Unfortunately this
 249 critical ^{60}Fe abundance is intermediate in the range of current best estimates
 250 (Chen et al., 2009; Mishra et al., 2010; Quitte et al., 2010; Telus et al., 2011;
 251 Spivak-Birndorf et al., 2011; Tang and Dauphas, 2011). As such, it is difficult
 252 to determine the relative importance of latent heat release without a well-
 253 constrained ^{60}Fe abundance. Nevertheless, a release of 270 kJ/kg of latent
 254 heat could increase temperatures by up to several hundred Kelvin (assuming
 255 no conductive loss of heat and a heat capacity of 400 J/kg/K) and, like any
 256 additional heat source, would prolong cooling. For all models presented here,
 257 the temperature-independent specific heat is near the lower limit for metallic
 258 iron and thus hastens cooling (Ghosh and McSween, 1999).

259 To quantify the effects of an insulating mantle we have run a series of
 260 simulations for a 50-km body with $^{60}\text{Fe}/^{56}\text{Fe} = 4 \times 10^{-7}$ and a surface layer

261 with low thermal diffusivity. These calculations suggest that a silicate mantle
262 (thermal conductivity = 2 W/m/K, heat capacity = 1200 J/kg/K) thicker
263 than ~ 0.5 km would prevent rapid cooling > 1000 K/Myr for nearly all radii.
264 With an initially chondritic composition, the core should be of order 40%
265 of the radius, i.e. 20 km in this example, overlain by a mantle ~ 30 km
266 thick (Haack et al., 1990). Therefore, any reasonable thickness for a silicate
267 mantle would prevent the rapid cooling rates (> 1000 K/Myr) measured for
268 some IVAs. This argues strongly in favor of a collision exposing the IVA core
269 before it cooled below 1000 K (Yang et al., 2007).

270 We have performed a similar calculation for a surface regolith (thermal
271 conductivity = 0.01 W/m/K, heat capacity = 1200 J/kg/K) in place of a
272 mantle (Haack et al., 1990). A regolith thicker than ~ 50 m would reduce the
273 range of cooling rates to below that measured for the IVAs. For the range of
274 regolith and mantle thickness considered, 0-0.5 km and 0-5 km respectively,
275 the dominant effect on the thermal evolution is a reduction of the highest
276 cooling rates at the base of the insulating layer. These insulating layers
277 do not influence central cooling rates until they become sufficiently thick
278 (approximately 0.5 km and 5 km respectively) such that the timescale over
279 which they conductively transfer heat becomes comparable to the timescale
280 of conductive heat loss across the whole of the 50-km metallic core.

281 Neglecting the release of latent heat, the temperature dependence of spe-
282 cific heat, and the effect of an insulating layer, act to hasten the loss of
283 thermal energy and thus artificially increase interior cooling rates. Since the
284 slowest IVA cooling rates are most difficult to reproduce in a mantle-free
285 body, treatment of these phenomena could extend the estimated range of

286 possible parent bodies to sizes less than $R=50$ km.

287 Our model does not treat the convection of molten material, which would
288 occur for melt fractions $> 50\%$. For the Fe-Ni-S system, the assumed initial
289 temperature of 1750 K would correspond to high degrees of partial melting.
290 The details of convective processes in an exposed molten core are not well
291 understood and are beyond the scope of this study. Convection in such a
292 system would increase the rate of heat loss from the interior and perhaps
293 require larger bodies to ensure ~ 100 K/Myr cooling near the center.

294 *5.2. Initial and Boundary Temperatures*

295 The ability of our model to reproduce the IVA cooling rates is unaffected
296 by changes to initial temperatures down to 1000 K and nebular temperatures
297 up to 300 K. For instance, the range of cooling rates during the formation
298 of the Widmanstätten pattern (1000-700 K) from the center to $0.9R$ for
299 the $R=50$ km body in Figure 2A is 140-8500 K/Myr. Reducing the initial
300 temperature of this body from 1750 K to 1000 K changes this range to 140-
301 16000 K/Myr, only the fastest cooling rates near the surface are affected. The
302 reason for the increase in cooling rates at the upper end of this range is due to
303 our focus on the narrow range of temperatures at which the Widmanstätten
304 pattern forms. In other words, the lowering of initial temperature shifts the
305 curves in Figure 2 downwards, which causes a wider range of rates between
306 1000-700 K. Increasing the boundary temperature up to a plausible maximum
307 of 300 K (Yang et al., 2007) also has little effect on cooling rates and results
308 in a range of 110-6500 K/Myr for the above example. The thermal model of
309 Yang et al. (2008) is similarly insensitive to changes in initial and boundary
310 temperatures.

311 5.3. *U-Pb Closure Temperature*

312 These models assume a U-Pb closure temperature of 600 K, however
313 this value is not well constrained. Blichert-Toft et al. (2010) suggest 573 K
314 based on the assumption that the closure temperature of Pb in sulfides is
315 the same as that of Os. Studies of U and Pb diffusion in silicates suggest
316 closure temperatures of about 625 ± 50 K (Spear and Parrish, 1996). This
317 suggests that our adopted closure temperature of 600 K may be accurate
318 to approximately ± 100 K, but specific measurements of U/Pb diffusion in
319 sulfides at elevated temperatures are essential for interpreting the U-Pb ages
320 of iron meteorites. This uncertainty predominantly affects the calculated
321 closure ages in Figure 3. For example, a lower closure temperature of 500 K
322 demands a slightly smaller body (approximately 50 km rather than 55 km
323 when $^{60}\text{Fe}/^{56}\text{Fe} = 4 \times 10^{-7}$) to match the age constraint for Muonionalusta.
324 This difference is insignificant relative to other uncertainties in the model.

325 5.4. *Precision of U-Pb Ages*

326 We have assumed that the closure age of Muonionalusta is 4565.3 ± 0.1
327 Ma (Blichert-Toft et al., 2010). However, this value could be in error by
328 ~ 1 Myr due to variations in the $^{238}\text{U}/^{235}\text{U}$ value of CAIs (Amelin et al.,
329 2010). Ages younger by 1 Myr would permit larger parent bodies because
330 of the additional time available to reach U-Pb closure. Older ages would
331 require smaller bodies such that closure occurs even faster. Therefore, this
332 uncertainty translates into a slightly broader range of acceptable parent body
333 sizes. At the lower size limit this effect is insignificant, i.e. less than 5 km
334 difference from our standard assumption of CAI ages equal to 4567.7 Ma. At

335 the upper limit, a younger closure age for Muonionalusta could allow parent
336 bodies up to $R=125$ km.

337 5.5. *Effect of Delayed Accretion*

338 Hf-W chronometry and thermal modeling suggest that fractionally crys-
339 tallized iron meteorite parent bodies accreted within 1.5 Myr of CAI forma-
340 tion (Qin et al., 2008). We adopt this constraint as an upper limit to the
341 time of formation and use it to recalculate the results in Figures 2 and 3.
342 For Figure 2A, the range of cooling rates for radii inside of $0.9R$ are 140-
343 8500 K/Myr. Delaying accretion to 1.5 Myr has little effect on these rates,
344 it simply reduces the amount of live ^{60}Fe and produces a range of cooling
345 rates from 225-9000 K/Myr. Figure 2B is unaffected by the assumed time of
346 accretion due to a lack of ^{60}Fe . In short, later times of accretion primarily
347 act to dampen peak temperatures and have little influence on cooling rates
348 below 1000 K.

349 The size constraints for the IVA core are similarly unaffected by times of
350 accretion up to 1.5 Myr. Delayed accretion effectively shifts the curves in
351 Figure 3 upwards, producing no change in the upper limit for the core size.
352 In other words, the point of intersection of the $0.7R$ curve and the age of
353 Muonionalusta will never shift to larger radii with later times of accretion.
354 Delayed accretion also has little effect on the lower size limit. This insensitiv-
355 ity is a result of competing processes in cores heated by ^{60}Fe . With delayed
356 accretion less time is available to reach U-Pb closure, thus requiring faster
357 cooling to produce Muonionalusta at $0.7R$. But, less live ^{60}Fe is present to
358 prolong cooling. These two effects act to cancel out one another.

359 6. Conclusions

360 We have argued that the parent core of the iron IVA meteorites was
361 between 50 - 110 km in radius, dependent primarily on the abundance of
362 live ^{60}Fe incorporated into the core. Cores in this size range follow a crys-
363 tallization sequence that match constraints set by metallographic cooling
364 rates (Yang et al., 2007, 2008), a U-Pb age (Blichert-Toft et al., 2010) and
365 geochemical data (Rasmussen et al., 1995; Wasson and Richardson, 2001;
366 Ruzicka and Hutson, 2006; McCoy et al., 2011). An estimate of $R=150\pm50$
367 km by Yang et al. (2008) is consistent with the upper end of this size range,
368 though our models are also consistent with a IVA core up to three times
369 smaller. The lower gravity in a smaller parent may facilitate the trapping of
370 silicate inclusions in a molten core (Ruzicka and Hutson, 2006). The proba-
371 bility of near-catastrophic collisions necessary to expose a molten core should
372 be greater for smaller bodies (Bottke et al., 2005). The dependence of our
373 results on a single old age emphasizes the need for additional dating of Muo-
374 nionalusta and other IVAs. Experimental confirmation of Muonionalusta's
375 predicted cooling rates of ~ 500 K/Myr is equally important to future studies
376 on the thermal evolution of the IVA core.

377 The range of cooling rates for the IVAs is the greatest of any chemical
378 group (Haack and McCoy, 2005; Yang et al., 2006; Goldstein et al., 2009;
379 Yang et al., 2010), suggesting they represent one of the largest iron mete-
380 orite parent cores with measured rates. Determination of cooling rates for
381 currently unmeasured groups could reveal otherwise. With a radius between
382 50 - 110 km, the IVA core must have derived from a fully differentiated par-
383 ent body that was at least twice as large (Haack et al., 1990). However,

384 due to large uncertainties regarding the hit-and-run formation scenario, it is
 385 difficult to precisely estimate the size of the fully differentiated IVA parent
 386 body prior to the collision. Nevertheless, our results suggest that planetary
 387 bodies $\sim 200\text{-}500$ km in diameter were present during the first few Myr of
 388 solar system history, with a possibility of even larger bodies depending upon
 389 the details of the collision that exposed the IVA core and the currently un-
 390 known cooling rates of other iron groups. This removes the necessity, though
 391 does not preclude the possibility of 10^3 km, proto-planetary bodies early in
 392 solar system history (Yang et al., 2008).

393 For this scenario of formation within an exposed core, IVAs with fast
 394 cooling rates (>1000 K/Myr) may have absolute ages separated by as little
 395 as a few times 10^5 years from CAI formation (Table 1). Confirmation of this
 396 would provide important clues to understanding the timescales involved in
 397 the formation of the first planetary bodies in the solar system.

398 Though Muonionalusta experienced shock melting, one of its troilite grains
 399 somehow preserved the old age measured by Blichert-Toft et al. (2010). If
 400 similar troilite grains can be dated in other IVAs, then the resulting range
 401 of U-Pb closure ages will provide a tighter constraint on the size of the IVA
 402 parent. For example, the range of closure ages for an $R=50$ -km core is less
 403 than half that of an $R=100$ -km core (Fig. 3). The core sizes of other frac-
 404 tionally crystallized iron groups with diverse cooling rates, such as the IIAB,
 405 IIIAB and IVBs (Yang et al., 2008, 2010), can be constrained by modeling
 406 both cooling rates and U-Pb ages, assuming such ages can be measured.

407 Previous studies on the formation and crystallization of fractionally crys-
 408 tallized irons assumed that the thermal effects of ^{60}Fe were insignificant. This

409 is reasonable for irons that formed inside of cores surrounded by insulating
 410 mantles since they would crystallize after ^{60}Fe was largely extinct. However,
 411 the age of Muonionalusta suggests that mantle-free cores may have crystal-
 412 lized when ^{60}Fe was still extant. As we have shown, cooling rates can be
 413 affected by the decay of this isotope. Unfortunately, current uncertainties in
 414 its initial abundance make it difficult to specifically quantify the relevance
 415 of ^{60}Fe decay to the thermal evolution of these parent bodies. If ^{60}Fe was
 416 present during the crystallization of iron groups like the IVA, IIAB, IIIAB
 417 and IVBs, then updated models will result in a reduction of the inferred sizes
 418 of these parent bodies.

419

420 **Acknowledgements** We thank Eric Gaidos and Rick Carlson for helpful
 421 comments regarding this study. Ed Scott, Joe Goldstein and an anonymous
 422 referee provided thoughtful reviews that led to significant improvement of
 423 this manuscript. NAM acknowledges support from the Carnegie Institution
 424 of Washington and the NASA Astrobiology Institute. This work was in part
 425 supported by NASA Cosmochemistry grant NNX10AG94G to RJW.

426 References

- 427 Amelin, Y., Kaltenbach, A., Iizuka, T., Stirling, C.H., Ireland, T.R., Pataev,
 428 M., Jacobsen, S., 2010. U-Pb chronology of the Solar System's oldest solids
 429 with variable $^{238}\text{U}/^{235}\text{U}$. *Earth. Planet. Sci. Lett.* 300, 343-350.
- 430 Asphaug, E., Agnor, C.B., Williams, Q., 2006. Hit-and-run planetary colli-
 431 sions. *Nature* 439, 155-160.

432 Blichert-Toft, J., Moynier, F., Lee, C. A., Telouk, P., Albarede, F., 2010.
 433 The early formation of the IVA iron meteorite parent body. *Earth Planet.*
 434 *Sci. Lett.* 296, 469-480.

435 Bottke, W.F., Durda, D.D., Nesvorny, D., Jedicke, R., Morbidelli, A.,
 436 Vokrouhlicky, D., Levison, H.F., 2005. Linking the collisional history of
 437 the main asteroid belt to its dynamical excitation and depletion. *Icarus*
 438 179, 63-94.

439 Burkhardt, C., Kleine, T., Bourdon, B., Palme, H., Zipfel, J., Friedrich,
 440 J.M., Ebel, D.S., 2008. Hf-W mineral isochron for Ca,Al-rich inclusions:
 441 Age of the solar system and the timing of core formation in planetesimals.
 442 *Geochim. Cosmochim. Acta* 72, 6177-6197.

443 Chabot, N.L., Haack, H., 2005. Evolution of asteroidal cores, in Lauretta,
 444 D.S., McSween, H.Y. (Eds.), *Meteorites and the Early Solar System II*,
 445 University of Arizona Press, Tucson, pp. 747-771.

446 Chen, J.H., Papanastassiou, D.A., Wasserburg, G.J., 2009. A search for
 447 nickel isotopic anomalies in iron meteorites and chondrites. *Geochim. Cos-*
 448 *mochim. Acta* 73, 1461-1471.

449 Dauphas, N., Cook, D.L., Sacarabany, A., Frohlich, C., Davis, A.M., Wad-
 450 hwa, M., Pourmand, A., Rauscher, T., Gallino, R., 2008. Iron 60 evidence
 451 for early injection and efficient mixing of stellar debris in the protosolar
 452 nebula. *Astrophys. J.* 686, 560-569.

453 Ghosh, A., McSween, H.Y., 1998. A thermal model for the differentiation of
 454 asteroid 4 Vesta based on radiogenic heating. *Icarus* 134, 187-206.

455 Ghosh, A., McSween, H.Y., 1999. Temperature dependence of specific heat
456 capacity and its effect on asteroid thermal models. *Meteorit. Planet. Sci.*
457 34, 121-127.

458 Goldstein, J.I., Scott, E.R.D., Chabot, N.L., 2009. Iron meteorites: Crys-
459 tallization, thermal history, parent bodies and origin. *Chemie der Erde -*
460 *Geochemistry* 69, 293-325.

461 Haack, H., Rasmussen, K.L., Warren, P.H., 1990. Effects of re-
462 golith/megaregolith insulation on the cooling histories of differentiated
463 asteroids. *J. Geophys. Res.* 95, 5111-5124.

464 Haack, H., Scott, E.R.D., 1992. Asteroid core crystallization by inward den-
465 dritic growth. *J. Geophys. Res.* 97, 14727-14734.

466 Haack, H., Scott, E.R.D., Love, S.G., Brearley, A.J., McCoy, T.J., 1996.
467 Thermal histories of IVA stony-iron and iron meteorites: Evidence for
468 asteroid fragmentation and reaccretion. *Geochim. Cosmochim. Acta* 60,
469 3103-3113.

470 Haack, H., McCoy, T.J., 2005. Iron and stony-iron meteorites, in Holland,
471 H.D., Turekian, K.K. (Eds.), *Meteorites, Comets and Planets, Treatise on*
472 *Geochemistry*, Volume 1, Elsevier-Pergamon, Oxford, pp. 325-347.

473 Hevey, P.J., Sanders, I.S., 2006. A model for planetesimal meltdown by ^{26}Al
474 and its implications for meteorite parent bodies. *Meteorit. Planet. Sci.* 41,
475 95-106.

476 Jacobsen, B., Yin, Q., Moynier, F., Amelin, Y., Krot, A.N., Nagashima, K.,
477 Hutcheon, I.D., Palme, H., 2008. ^{26}Al - ^{26}Mg and ^{207}Pb - ^{206}Pb systematics of

478 Allende CAIs: Canonical solar initial $^{26}\text{Al}/^{27}\text{Al}$ reinstated. *Earth. Planet.*
 479 *Sci. Lett.* 272, 353-364.

480 Johansen, A., Oishi, J.S., Mac Low, M., Klahr, H., Henning, T., Youdin,
 481 A., 2007. Rapid planetesimal formation in turbulent circumstellar disks.
 482 *Nature* 448, 1022-1025.

483 Keil, K., Stöffler, D., Love, S.G., Scott, E.R.D., 1997. Constraints on the
 484 role of impact heating and melting in asteroids. *Meteorit. Planet. Sci.* 32,
 485 349-363.

486 Kleine, T., Mezger, K., Palme, H., Scherer, E., Munker, C., 2005. Early core
 487 formation in asteroids and late accretion of chondrite parent bodies: Evi-
 488 dence from ^{182}Hf - ^{182}W in CAIs, metal-rich chondrites, and iron meteorites.
 489 *Geochim. Cosmochim. Acta* 69, 5805-5818.

490 McCoy, T.J., Walker, R.J., Goldstein, J.I., Yang, J., McDonough, W.F.,
 491 Rumble, D., Chabot, N.L., Ash, R.D., Corrigan, C.M., Michael, J.R., Ko-
 492 tula, P.G., 2011. Group IVA irons: New constraints on the crystallization
 493 and cooling history of an asteroidal core with a complex history. *Geochim.*
 494 *Cosmochim. Acta*, in revision.

495 McKeegan, K.D., Davis, A.M., 2005. Early solar system chronology, in Hol-
 496 land, H.D., Turekian, K.K. (Eds.), *Meteorites, Comets and Planets, Trea-*
 497 *tise on Geochemistry*, Volume 1, Elsevier-Pergamon, Oxford, pp. 431-460.

498 Mishra, R.K., Goswami, J.N., Tachibana, S., Huss, G.R., Rudraswami, N.G.,
 499 2010. ^{60}Fe and ^{26}Al in chondrules from unequilibrated chondrites: Implica-
 500 tions for early solar system processes. *Astrophys. J. Lett.* 714, L217-L221.

501 Mittlefehldt, D.W., McCoy, T.J., Goodrich, C.A., Kracher, A., 1998. Non-
502 chondritic meteorites from asteroidal bodies, in: Papike. J.J. (Ed.), Plan-
503 etary Materials, Reviews in Mineralogy, Volume 36. Mineralogical Society
504 of America, Washington, ch. 4.

505 Moskovitz, N.M., Gaidos, E., 2011. Differentiation of planetesimals and the
506 thermal consequences of melt migration. *Meteorit. Planet. Sci.* in press.

507 Ogliore, R.C., Huss, G.R., Nagashima, K., 2011. The problem of bias in mass
508 spectrometry ratio estimation (abstract #1592). 42nd Lunar and Planetary
509 Science Conference. CD-ROM.

510 Qin, L., Dauphas, N., Wedhwa, M., Masarik, J., Janney, P.E. Rapid accretion
511 and differentiation of iron meteorite parent bodies inferred from ^{182}Hf - ^{182}W
512 chronometry and thermal modeling. *Earth Planet. Sci. Lett.* 273, 94-104.

513 Quitte, G., Markowski, A., Latkoczy, C., Gabriel, A., Pack, A., 2010. Iron-60
514 heterogeneity and incomplete mixing in the early solar system. *Astrophys.*
515 *J.* 720, 1215-1224.

516 Rasmussen, K.L., Ulff-Moller, F., Haack, H., 1995. The thermal evolu-
517 tion of IVA iron meteorites: Evidence from metallographic cooling rates.
518 *Geochim. Cosmochim. Acta* 59, 3049-3059.

519 Rugel, G., Faestermann, T., Knie, K., Korschinek, G., Poutivtsev, M., Schu-
520 mann, D., Kivel, N., Gunther-Leopold, I., Weinreich, R., Wohlmuther, M.,
521 2009. New measurements of the ^{60}Fe half-life. *Phys. Rev. Lett.* 103, 072502.

522 Ruzicka, A., Hutson, M., 2006. Differentiation and evolution of the IVA

523 meteorite parent body: Clues from pyroxene geochemistry in the Steinbach
524 stony-iron meteorite. *Meteorit. Planet. Sci.* 41, 1959-1987.

525 Scott, E.R.D., Haack, H., McCoy, T.J., 1996. Core crystallization and
526 silicate-metal mixing in the parent body of the IVA iron and stony-iron
527 meteorites. *Geochim. Cosmochim. Acta* 74, 1615-1631.

528 Spear, F.S., Parrish, R.R., 1996. Petrology and cooling rates of the Valhalla
529 Complex, British Columbia, Canada. *J. Petrology* 37, 733-765.

530 Spivak-Birndorf, L.J., Wadhwa, M., Janney, P.E., 2011. ^{60}Fe - ^{60}Ni chronol-
531 ogy of the D-Orbigny angrite: Implications for the initial Solar System
532 abundance of ^{60}Fe (abstract #2281). 42nd Lunar and Planetary Science
533 Conference. CD-ROM.

534 Tachibana, S., Huss, G.R., Kita, N.T., Shimoda, G., Morishita, Y., 2006. ^{60}Fe
535 in chondrites: Debirs from a nearby supernova in the early solar system?
536 *Astrophys. J. Lett.* 639, L87-L90.

537 Tang, H., Dauphas, N., 2011. Constraints from achondrites on the initial
538 $^{60}\text{Fe}/^{56}\text{Fe}$ ratio of the Solar System (abstract #1068). 42nd Lunar and
539 Planetary Science Conference. CD-ROM.

540 Telus, M., Huss, G.R., Nagashima, K., Ogliore, R.C., Tachibana, S., Jilly,
541 C.E., 2011. Possible heterogeneity of ^{60}Fe in chondrules from primitive
542 ordinary chondrites (abstract #2559). 42nd Lunar and Planetary Science
543 Conference. CD-ROM.

544 Ulf-Møller, F., Rasmussen, K.L., Prinz, M., Palme, H., Spettel, B., Kalle-
545 meyn, G.W., 1995. Magmatic activity on the IVA parent body: Evidence

546 from silicate-bearing iron meteorites. *Geochim. Cosmochim. Acta* 59, 4713-
547 4728.

548 Wadhwa, M., Amelin, Y., Bogdanovski, O., Shukolyukov, A., Lugmair,
549 G.W., Janney, P., 2009. Ancient relative and absolute ages for a basaltic
550 meteorite: Implications for timescales of planetesimal accretion and differ-
551 entiation. *Geochim. Cosmochim. Acta* 73, 5189-5201.

552 Walker, R.J., McDonough, W.F., Honesto, J., Chabot, N.L., McCoy, T.J.,
553 Ash, R.D., Bellucci, J.J., 2008. Modeling fractional crystallization of group
554 IVB iron meteorites. *Geochim. Cosmochim. Acta* 72, 2198-2216.

555 Wasson, J.T., Richardson, J.W., 2001. Fractionation trends among IVA iron
556 meteorites: Contrasts with IIIAB trends. *Geochim. Cosmochim. Acta* 65,
557 951-970.

558 Wasson, J.T., Matsunami, Y., Rubin, A.E., 2006. Silica and pyroxene in IVA
559 irons; possible formation of the IVA magma by impact melting and reduc-
560 tion of L-LL-chondrite materials followed by crystallization and cooling.
561 *Geochim. Cosmochim. Acta* 70, 3149-3172.

562 Willis, J., Wasson, J.T., 1978. Cooling rates of group IVA iron meteorites.
563 *Earth Planet. Sci. Lett.* 40, 141-150.

564 Yang, J., Goldstein, J.I., 2006. Metallographic cooling rates of the IIIAB iron
565 meteorites. *Geochim. Cosmochim. Acta* 70, 3197-3215.

566 Yang, J., Goldstein, J.I., Scott, E.R.D., 2007. Iron meteorite evidence for
567 early formation and catastrophic disruption of protoplanets. *Nature* 446,
568 888-891.

- 569 Yang, J., Goldstein, J.I., Scott, E.R.D., 2008. Metallographic cooling rates
570 and origin of IVA iron meteorites. *Geochim. Cosmochim. Acta* 72, 3043-
571 3061.
- 572 Yang, J., Goldstein, J.I., Michael, J.R., Kotula, P.G., Scott, E.R.D., 2010.
573 Thermal history and origin of the IVB iron meteorites and their parent
574 body. *Geochim. Cosmochim. Acta* 74, 4493-4506.

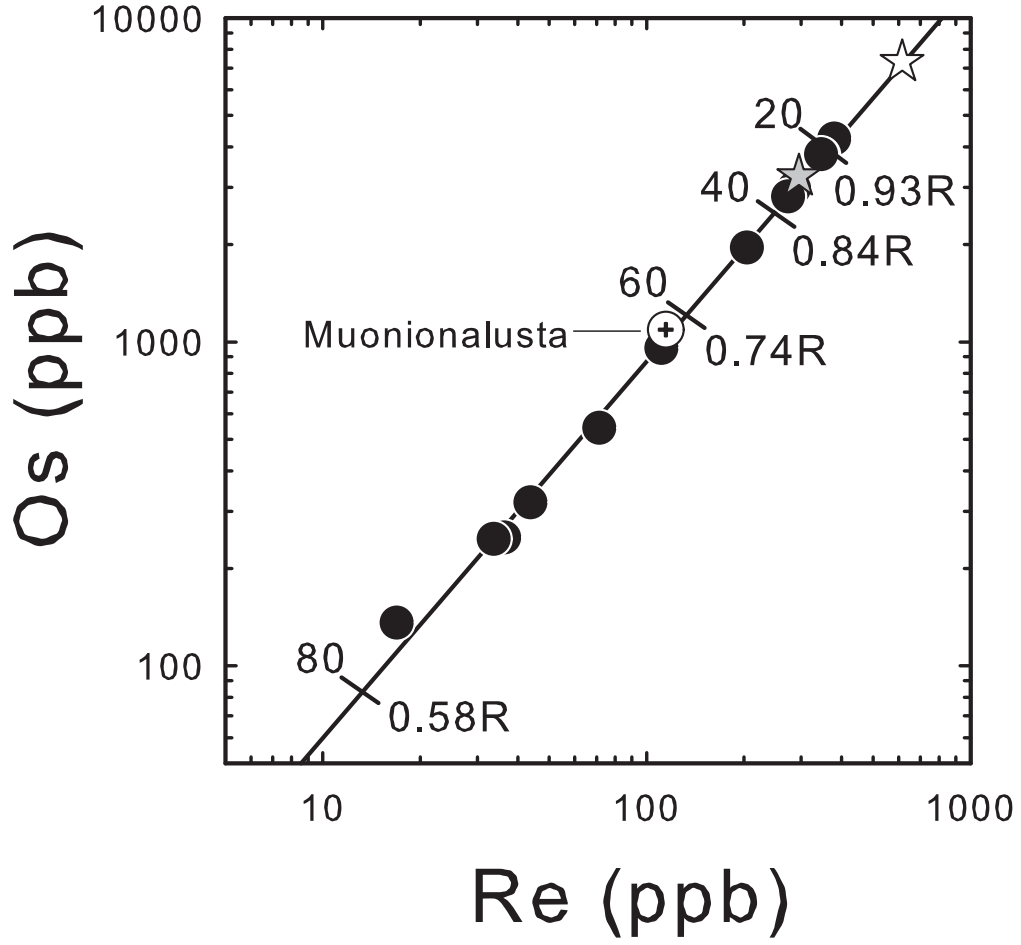


Figure 1: Plot of Re versus Os (in ppb) for 14 group IVA iron meteorites. Muonionalusta is shown by the open circle with a cross. The solid line is the fractional crystallization trend for 50:50 mixes of equilibrium solids and liquids, using parameters discussed in the text. Tick marks indicate 20 through 80% extents of fractional crystallization (equivalent to 0.58-0.93R in an inwardly crystallizing metallic core). For this model, Muonionalusta is produced after $\sim 60\%$ fractional crystallization. The grey star represents the assumed initial liquid composition; the open star denotes the composition of the first solid to form from this liquid.

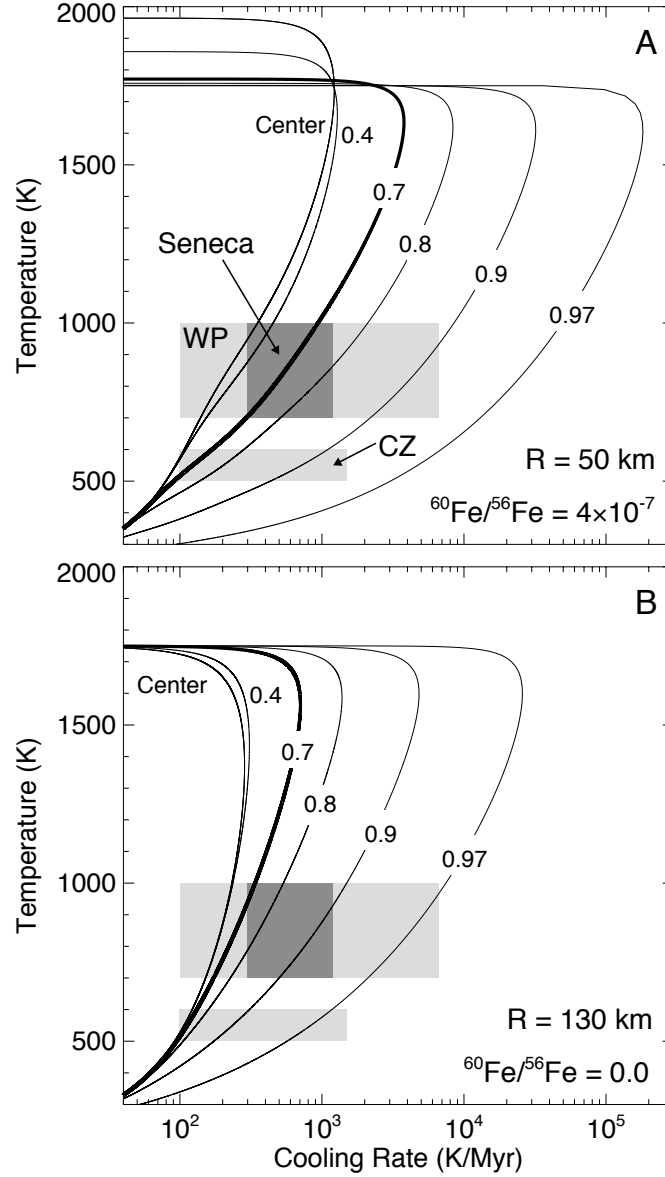


Figure 2: Cooling rate versus temperature at different depths, expressed as fractions of the parent radius, in exposed cores with maximal ^{60}Fe (A) and in the absence of ^{60}Fe (B). The light grey regions represent temperatures and measured IVA cooling rates during formation of the Widmanstätten pattern (WP) and cloudy zone particles (CZ). The dark grey box represents the measured cooling rates for Seneca Township, a sample with similar Ni-content to Muonionalusta. In each case the sizes of the cores have been adjusted such that the measured ranges of WP and CZ rates are reproduced, and so that a radius of 0.7R crystallizes at the rates measured for Seneca. These two examples represent upper ($R=130$ km) and lower ($R=50$ km) limits to the size of the IVA core.

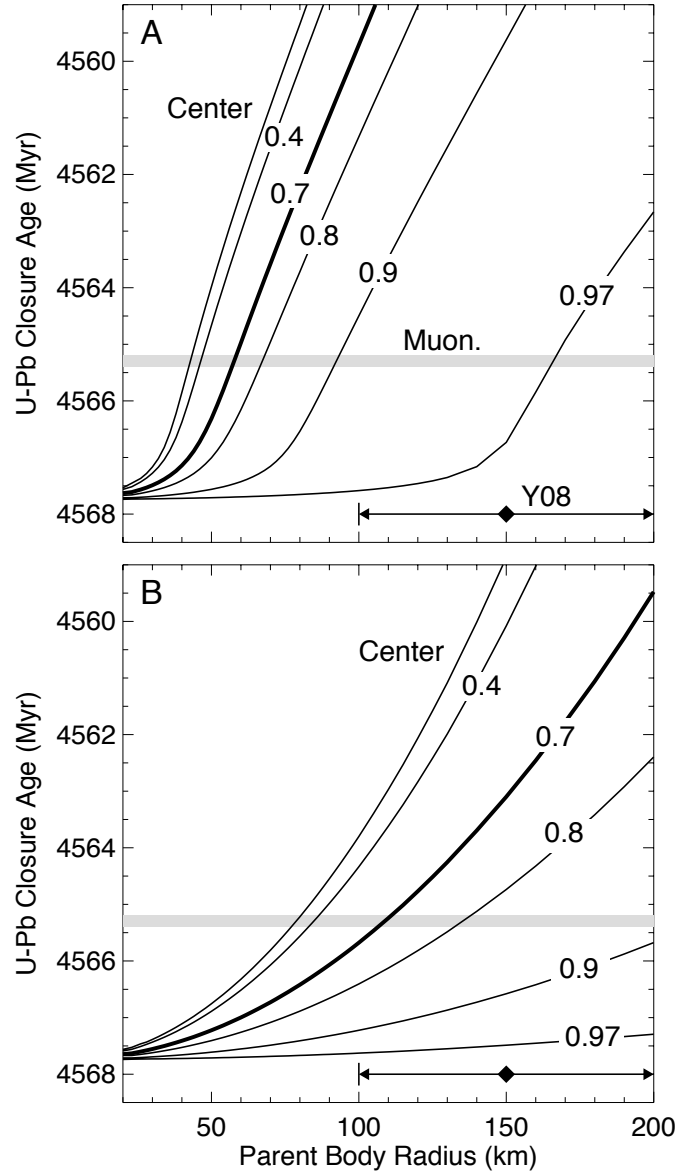


Figure 3: U-Pb closure ages at different depths for a range of parent body sizes with initial $^{60}\text{Fe}/^{56}\text{Fe}=4 \times 10^{-7}$ (panel A) and $^{60}\text{Fe}/^{56}\text{Fe}=0$ (panel B). The thick curve (0.7R) represents the expected radius of Muonionalusta's origin. The grey region denotes Muonionalusta's closure age of 4565.3 ± 0.1 Ma. The size estimate for the IVA parent body from Yang et al. (2008) is shown at the bottom right. The closure age at the formation radius of Muonionalusta is reproduced for core radii between 50 (panel A) and 110 km (panel B), depending upon the initial abundance of ^{60}Fe .

Meteorite	Cooling Rate ^a (K/Myr)	Predicted U-Pb Closure Age (Ma)
La Grange	6600	4567.5
Obernkirchen	2900	4567.4
Bishop Canyon	2500	4567.4
Jamestown	1900	4567.3
Gibeon	1500	4567.2
Seneca Township	580	4566.4
Altonah	420	4565.8
Muonionalusta	290-940 ^b	4565.3±0.1 ^c
Bushman Land	260	4564.5
Duel Hill	220	4564.0
Steinbach	150	< 4564
New Westville	120	< 4564
Chinaulta	110	< 4564
Duchesne	100	< 4564

Table 1: Cooling rates and U-Pb closures ages for a IVA core with R=50 km and $^{60}\text{Fe}/^{56}\text{Fe}=4 \times 10^{-7}$

^a Yang et al. (2008)

^b Model prediction

^c Blichert-Toft et al. (2010)